

<https://doi.org/10.1038/s40494-026-02428-4>

Exploring city-level climate risks for immovable cultural heritage in Beijing



Huimin Li & Ruqi Li

Climate change is increasingly threatening immovable cultural heritage. This study develops a climate risk assessment framework to evaluate risks across 3619 immovable cultural heritage sites in Beijing. The results show that mean risk under the high-emission scenario (SSP5-8.5) is approximately 41.5% higher than under the medium-emission scenario (SSP2-4.5). Climate risks generally decline from national to municipal, district, and district surveyed heritage; yet lower level heritage categories are more vulnerable and exhibit a significantly greater risk increase when shifting from SSP2-4.5 to SSP5-8.5. Spatially, high risk areas concentrate primarily in central urban districts and the western mountainous regions. The relative risk gradient remains robust despite uncertainty. Based on these findings, this study highlights three policy implications for adapting cultural heritage to climate change: strengthening greenhouse gas mitigation to reduce climate hazards; developing proactive adaptation plans to reduce vulnerability; and implementing differentiated measures to address resource constraints.

Climate change is intensifying, placing global cultural heritage under unprecedented threats^{1–3}. Extreme heat, increased frequency of heavy rainfall, seasonal climatic reversals, and compound geological hazards are profoundly altering the environmental stability and physical integrity of cultural heritage^{4–6}. Immovable cultural heritage, particularly ancient buildings and monuments exposed in open spaces, are highly sensitive and irreversible, making them vulnerable frontlines under climate change impact^{7–9}. The UNESCO (United Nations Educational, Scientific, and Cultural Organization) and the IPCC (Intergovernmental Panel on Climate Change) have emphasized that cultural heritage is a critical component of the “non-economic climate risk” identification system and should be integrated into the global climate adaptation strategy framework^{10–12}.

While the impacts of climate change are globally widespread, the spatial heterogeneity of these impacts on urban-scale cultural heritage, especially in megacities, remains underexplored¹³. In recent years, researchers worldwide have increasingly investigated the compound stress mechanisms of regional climates on heritage materials, structures, and functions, such as heat-induced shrinkage and cracking in wooden heritage, accelerated weathering and seepage in masonry due to extreme precipitation, and stress accumulation from freeze–thaw cycle^{14,15}. Moreover, greater emphasis has been placed on the effects of air pollution on cultural heritage, leading to the development of several integrated approaches to assess air pollution threats to cultural heritage^{16–18}. However, existing studies have predominantly focused on World Heritage Sites or naturally exposed

archeological sites²⁹, leaving a critical gap in understanding of city-level climate risks to cultural heritage.

From a theoretical modeling perspective, climate risk assessment frameworks for cultural heritage are transitioning from predominantly qualitative descriptions to more quantitative and spatially explicit approaches. Early studies largely relied on case-based analyses or expert scoring to identify risk factors, often lacking systematic weighting schemes and fine-scale spatial representation^{19–21}. In recent years, the integration of GIS techniques, multi-source climate datasets, and indicator-based weighting methods, most notably the Analytic Hierarchy Process (AHP) and the Entropy Weight Method (EWM), has enabled a shift from single heritage site assessments toward city-wide risk assessment frameworks. This transition has been further supported by the increasing availability of CMIP6 climate scenarios and high-resolution downscaled simulations, enabling projections of cultural heritage risks under alternative future climate pathways such as SSP2-4.5 and SSP5-8.5^{22–24}.

Alongside these developments, methodological advances in broader climate risk research, particularly machine learning, have informed discussions in the heritage field. Supervised learning models such as Random Forest and XGBoost have been widely applied in data-rich hazard contexts (e.g. floods and landslides) to capture nonlinear relationships between hazard drivers and observed impacts^{25,26}. However, for cultural heritage climate risk assessment, the applicability of data-intensive machine learning methods remains constrained by the scarcity of long-term, site-specific damage observations and by the need for transparent, interpretable results

Beijing Climate Change Response Research and Education Center, Beijing University of Civil Engineering and Architecture, Beijing, China.

 e-mail: lihm@bucea.edu.cn

that can directly support conservation planning and governance^{27,28}. From the perspective of practicality, indicator-based frameworks grounded in expert knowledge, particularly hybrid approaches integrating AHP and EWM, continue to represent a pragmatic and operationally feasible choice for forward-looking, city-scale cultural heritage climate risk assessments, effectively balancing methodological rigor with decision-oriented interpretability²⁹.

In summary, existing literature still warrants further discussion in three key aspects: (1) Spatial scales. Most studies have been conducted at the heritage site level, whereas urban-scale cultural heritage climate risk assessments remain relatively scarce^{30,31}. Large-scale assessments can reveal regional heterogeneity and enable cross-site comparisons of risk levels. (2) Time scales. Current research places greater emphasis on cultural heritage vulnerability than on the characterization of future climate hazards, thereby limiting the capacity to project future risks under changing climatic conditions^{32,33}. (3) Risk management pathways. Climate risk research has not yet been fully integrated into cultural heritage protection practices, constraining its ability to deliver actionable guidance for prioritizing conservation interventions at the local level^{28,34}.

Beijing, as one of China's most densely populated megacities with a high concentration and diversity of cultural heritage, hosts more than 3600 immovable cultural heritage sites, including ancient architecture, archaeological sites, tombs, stone carvings, and modern historical landmarks. These heritages are distributed along a complex foothill-plain-urban fringe ecological gradient, exhibiting highly heterogeneous responses to extreme climate events. Under the combined effects of urban heat islands, changing precipitation patterns, and human interventions, the climate exposure of Beijing's cultural heritage continues to increase, necessitating the development of a systematic risk assessment and adaptation framework. This study proposes a comprehensive cultural heritage climate risk assessment framework that integrates the three dimensions of hazard, vulnerability, and exposure, leveraging high-resolution CMIP6 climate scenario data and specifically designed for city-scale immovable cultural heritage. By combining GIS-based spatial overlay analysis with multi-indicator weighting methods, the study systematically identifies spatial patterns of climate risk across Beijing's heritage assets, differentiated by conservation grade, geographic location, and material composition, reveals dominant risk drivers, and highlights priority zones and strategic pathways for adaptive governance and targeted intervention.

This study makes three key contributions: (1) Mapping the distribution of cultural heritage risks across the urban landscape, revealing distinct regional variations in climate risk and enabling systematic comparisons among different heritage assets; (2) Highlighting the cumulative climate risk posed by lower-grade heritage sites. While individually less prominent, these assets constitute the majority of heritage locations in megacities and collectively represent a substantial yet frequently overlooked component of urban climate vulnerability; (3) Establishing a replicable methodology for city-scale cultural heritage climate risk assessment by integrating a modular indicator framework with widely accessible geospatial datasets. Beyond Beijing, the framework is transferable to other heritage-dense metropolitan contexts, such as London, Rome, and Tokyo.

The paper is structured as follows: Section 2 presents the materials and methods; Section 3 details the risk modeling process from the perspectives of hazard, vulnerability, and exposure; Section 4 presents the results of the climate risks assessment; Section 5 discusses the policy implications; and Section 6 summarizes the main conclusions.

Methods

Study area

Beijing is a world-renowned historical and cultural city, boasting over 3000 years of urban development and more than 800 years of history as the national capital. It ranks among the Chinese cities with the highest number of World Heritage Sites and the greatest concentration of cultural relics. According to *the Law of the People's Republic of China on the Protection of Cultural Relics*³⁵, immovable cultural relics are classified into six categories:

sites of ancient culture (SOAC), ancient tombs (AT), ancient architectural structures (AAS), cave temples and stone carvings (CTASC), important modern and contemporary historic sites and typical buildings (IMACHSTB), and murals. The first five categories are predominantly exposed to outdoor environmental conditions, whereas murals are generally located indoors and thus less susceptible to direct climate-change-induced environmental stressors. Consequently, this study focuses on these five outdoor heritage categories.

A total of 3619 immovable cultural heritage sites are included in the analysis, distributed across 16 administrative districts characterized by alternating plains, hills, and mountains under a temperate monsoon climate with pronounced seasonality and inter-annual variability. These sites exhibit a distinct spatial pattern, with high concentrations observed in Dongcheng and Xicheng districts as well as in foothill transition zones, forming a clear "central concentration—peripheral dispersion" structure. China's immovable cultural relics are classified according to protection level into national-level, municipal-level, district-level, and district-wide surveyed heritage sites. Among the 3619 cultural heritage sites included in this study, 147 are designated at the national level, 263 at the municipal level, 789 at the district level, and 2420 fall under the category of district-wide surveyed cultural relics. To facilitate understanding of the spatial scope and classification framework applied in the subsequent risk assessment, Fig. 1 illustrates the overall spatial distribution of immovable cultural heritage in Beijing.

Research framework

To systematically assess the risks to Beijing's cultural heritage under the context of climate change, this study established a three-dimensional indicator system centered on "Hazard-Vulnerability-Exposure". The detailed methodological framework is illustrated in Fig. 2.

Risk assessment framework. The study employed the IPCC risk framework to quantify the climate risk of immovable cultural heritage in Beijing.

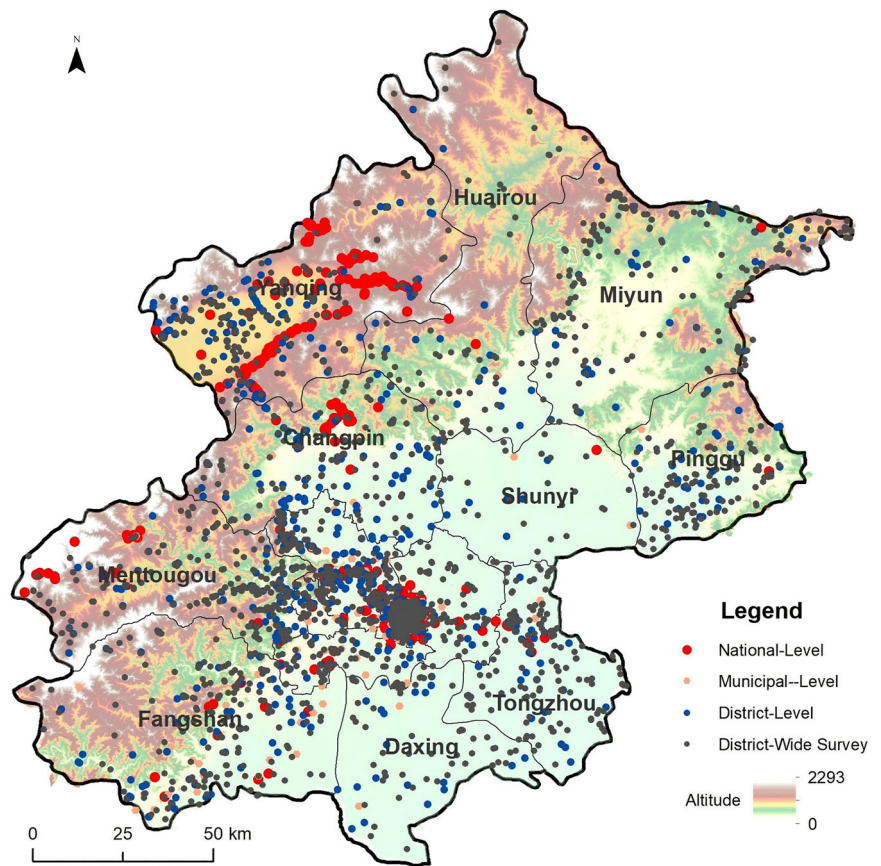
$$R = H * W_h + E * W_e + V * W_v \quad (1)$$

In the equation, R represents the climate change risk, H denotes the hazard of climate change, E represents the exposure of the elements at risk, and V denotes the vulnerability of the elements at risk. W_h , W_e , W_v are the respective weights of each component.

Risk assessment indicators. Based on a comprehensive review of existing research and data availability, this study selected 14 key indicators to represent the hazard, exposure, and vulnerability. The indicator system exhibits strong logical coherence with respect to data availability, spatial adaptability, and risk response mechanisms, thereby providing a robust foundation for the development of a city-scale climate risk assessment model for cultural heritage.

In the hazard dimension, emphasis was placed on capturing both the intensity and temporal characteristics of climatic factors relevant to cultural heritage deterioration. According to existing literature, climatic factors, including temperature, precipitation, wind, lightning, and freeze-thaw cycles, exert significant influences on the deterioration of cultural heritage^{36–39}. Climate-related risks arise not only from sudden and acute physical damage caused by extreme climatic events such as heavy rainfall and typhoons, but also from long-term shifts in key climatic variables such as temperature, precipitation, and humidity. These gradual changes contribute to accelerated deterioration through "dose-response" mechanisms, manifesting as flaking, blistering, cracking, color alteration, and rot^{39–41}. Climate risk assessments typically require long-term future climate projections. However, current climate models remain limited in their ability to reliably simulate phenomena such as wind patterns and lightning frequency over extended time scales. Therefore, this study focuses exclusively on temperature and precipitation as the two primary climatic variables. Annual

Fig. 1 | Spatial distribution map of cultural heritage in Beijing. This figure illustrates the geographical distribution of cultural heritage sites across different protection levels in Beijing, with the background colors depicting the city's topographical features.



mean temperature and annual mean precipitation were selected as representatives of long-term cumulative effects, reflecting thermal stress and moisture perturbation, respectively. Considering the pronounced abrupt impacts of extreme events on cultural heritage, maximum annual mean temperature and maximum annual mean precipitation were introduced as proxy variables for extreme heat and extreme precipitation.

In the exposure dimension, heritage value represents the social influence and historical significance of cultural heritage, with high-value sites generally exhibiting higher irreplaceability and greater potential losses, thus experiencing higher exposure. The Heritage scale reflects the physical spatial extent, where larger areas involve more pathways for climatic disturbances, resulting in more pronounced risk accumulation effects.

In the vulnerability dimension, intrinsic vulnerability is determined by the construction age and material composition of heritage sites. Construction age broadly reflects the duration of accumulated environmental exposure, with older structures generally exhibiting higher vulnerability. However, significant variations among individual cultural heritage sites may arise due to differences in materials and construction techniques. Traditional Chinese architectural craftsmanship, such as the dougong bracket system, often provides exceptional mechanical adaptability and resilience. Therefore, construction age should be regarded as a generalized proxy for long-term deterioration potential rather than an absolute determinant of intrinsic vulnerability. Material type influences thermal and moisture resistance as well as structural porosity; for instance, wood and rammed earth are highly sensitive to fluctuations in temperature and humidity.

Environmental vulnerability incorporates slope, distance to environmental risk points, vegetation cover, and land use type, collectively reflecting the capacity of the geographic environment to amplify or buffer climate hazards. Steep terrain, proximity to hazard points, and degraded ecosystems tend to exacerbate climatic impacts.

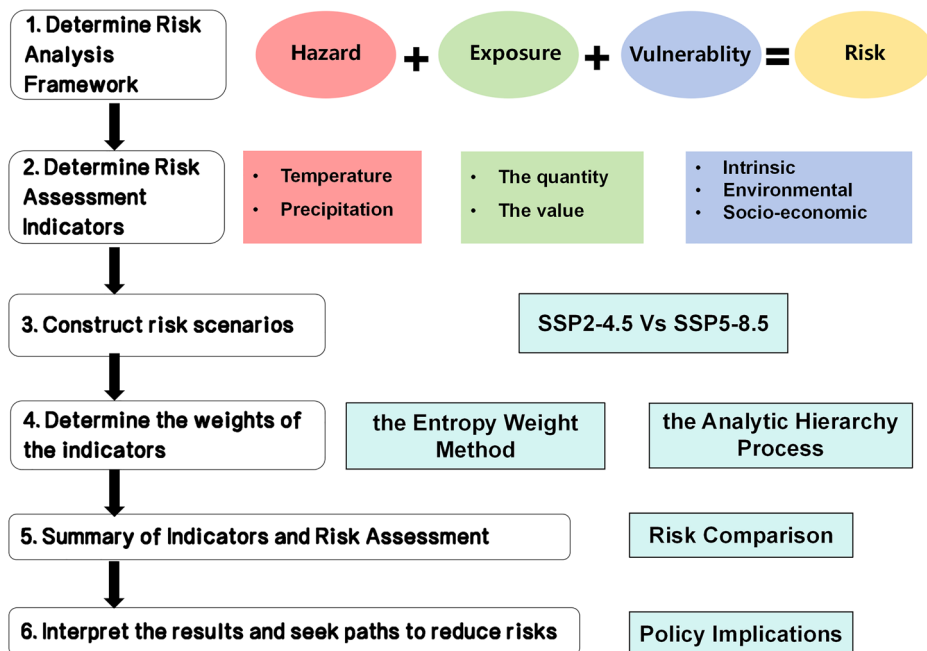
Regarding socioeconomic vulnerability, the fiscal revenue of the administrative region in which the heritage site is located serves as a proxy

for protective resource capacity, with higher revenue reflecting greater institutional capacity for management and maintenance, thereby contributing to reduced vulnerability. The population exerts a multifaceted influence on the vulnerability of cultural heritage. In densely populated areas, heritage sites often benefit from stronger community engagement in conservation efforts, yet they are simultaneously more susceptible to human-induced threats such as urban encroachment, tourism pressure, and infrastructure development. Conversely, sites in sparsely populated regions experience fewer anthropogenic disturbances but frequently lack institutional maintenance and monitoring, particularly for heritages with lower conservation grades, thereby increasing their exposure to natural degradation processes. This study employs population density within a 3-km radius as a proxy indicator for socio-cultural vulnerability. Higher population density within this buffer is associated with greater potential for local stewardship and thus reflects reduced human-related vulnerability.

Risk scenarios. This study selects two climate scenarios, SSP2-4.5 and SSP5-8.5, to assess risk disparities under different climatic conditions. SSP2-4.5 represents a moderate radiative forcing scenario, stabilizing at approximately 4.5 W/m² by 2100, which is widely regarded as a plausible future pathway. SSP5-8.5 corresponds to a high radiative forcing scenario, with forcing reaching up to 8.5 W/m² by 2100, and is generally considered to represent the upper bound of potential future climate change.

Weight of the indicators. This study employs a hybrid approach integrating both subjective and objective methodologies to determine indicator weights. In the hazard dimension, the Entropy Weight Method is employed to automatically assign indicator weights based on the sample distribution, ensuring both the distinguishability among climate disturbance variables and the objectivity of the weights. For other weights, it is challenging to compute them using purely objective weighting

Fig. 2 | The methodological framework for climate risk assessment of cultural heritage in Beijing. This figure presents a comprehensive overview of the methodological framework for climate risk assessment of cultural heritage in Beijing.



methods. In this study, the Analytic Hierarchy Process was employed to determine these weights. A pairwise comparison consistency matrix was constructed by conducting mutual evaluations of seven indicators using seven AI platforms—ChatGPT, Doubao, KIMI, Wenxin Yiyan, DeepSeek, Hailuo Wenwen, and Tongyi Qianwen—in order to enhance assessment accuracy. To ensure the comparability of the evaluations from each AI, a unified set of questions was presented to all platforms. As different AI models yielded distinct comparison matrices, their consistency was tested, typically using the following formula:

$$CI = \frac{\lambda_{\max}(A) - n}{n - 1} \tag{2}$$

In the equation, *CI* denotes the consistency index, *n* represents the order of the matrix, and $\lambda_{\max}(A)$ is the maximum eigenvalue of matrix *A*. When *CI* = 0, it indicates perfect consistency; the larger the *CI*, the greater the degree of inconsistency. To measure the magnitude of *CI*, the random consistency index (*RI*) is introduced, which is calculated using the same method as *CI*. On this basis, the random consistency ratio is then computed as follows:

$$CR = \frac{CI}{RI} \tag{3}$$

When *CR* < 0.1, the pairwise comparison matrix is considered to have satisfactory consistency, or its degree of inconsistency is deemed acceptable; otherwise, the matrix must be adjusted until satisfactory consistency is achieved. In this study, all AHP judgment matrices passed the consistency test. The results are shown in Table 1.

Data sources

This study employs both historical and projected climate data to evaluate the climate risk of cultural heritage sites in Beijing. Historical climate data (1901–2022) were obtained from the National Qinghai–Tibet Plateau Science Data Center (<https://data.tpdc.ac.cn/home>). The data have a spatial resolution of 1 km (0.008°) and a temporal resolution of monthly, covering temperature and precipitation variations across China^{42,43}. Future climate data (2021–2100) were also sourced from the National Qinghai–Tibet Plateau Science Data Center. The dataset is based on the CMIP6 multi-

model ensemble under three representative Shared Socioeconomic Pathways (SSP1-1.9, SSP2-4.5, and SSP5-8.5), simulated by global climate models including EC-Earth3, GFDL-ESM4, and MRI-ESM2-0. A Delta downscaling method was applied to achieve a 1 km resolution, with the period 1981–2010 used as the baseline for systematic bias correction^{43,44}.

The Exposure and Intrinsic vulnerability indicators were derived from the ‘Beijing Cultural Relics Map’ platform (<https://maptable.com/s/p/cnzodzkujocg/map>). The dataset includes geographical information, age information, and the types of heritage. Environmental vulnerability is quantified at the individual site scale using GIS, based on a 30 m resolution DEM from the European Space Agency’s Copernicus program (2022), Beijing geological hazard points (2019) and land-use data (2023) from the Chinese Academy of Sciences Resource and Environmental Science Data Center (<https://www.resdc.cn/data.aspx?DATAID=290>), and monthly NDVI indices (2023) from NASA (<https://www.earthdata.nasa.gov>). Socio-economic vulnerability is represented by population density at 1 km resolution from WorldPop and regional fiscal revenue in 2023 from the Beijing Statistical Yearbook (<https://nj.tjj.beijing.gov.cn/nj/main/2024-tjnj/zk/indexch.htm>).

Risk modelling process

Hazard. This study selects four indicators - annual mean temperature, maximum annual mean temperature, annual mean precipitation, and maximum annual mean precipitation - to analyze their spatial distributions and temporal trends under two emission scenarios: the intermediate scenario (SSP2-4.5) and the high-emission scenario (SSP5-8.5).

Figure 3 illustrates the comparison of temperature under different climate scenarios. During the historical period, the spatial pattern of annual mean temperature (Fig. 3a) displays a “higher in urban centers, lower in mountainous areas” distribution. The central districts (Dongcheng, Xicheng, and Chaoyang) generally exceed 14 °C, while the northwestern mountainous regions (Yanqing and Miyun) remain below 12 °C. Under the SSP2-4.5 scenario (Fig. 3b), these mountainous regions are projected to experience warming of approximately 3.0 °C; under the SSP5-8.5 scenario (Fig. 3c), temperatures increase generally exceed 3.5 °C, with localized areas surpassing 4.0 °C. The spatial heterogeneity of maximum annual mean temperature is even more pronounced. During the historical period (Fig. 3d), high temperature values are predominantly concentrated in the southeastern plain districts, including Tongzhou, Daxing, and Shunyi,

Table 1 | Indicator weights for climate risk assessment of cultural heritage in Beijing

Target Level	Weight	Criterion Level	Indicator Level	Weight	
Hazard	0.5209 (0.1620–0.7245)	Temperature	Average Temperature	0.0195	
			Temperature Extreme	0.6450	
		Precipitation	Average Precipitation	0.0634	
			Extreme Precipitation	0.2721	
Vulnerability	0.2479 (0.1630–0.3090)	Intrinsic vulnerability	Construction Age of the Heritage Site	0.2693 (0.0618–0.4025)	
			Material Composition of the Heritage Site	0.1857 (0.1300–0.2139)	
		Environmental vulnerability	Slope	0.1249 (0.0520–0.3284)	
			Distance to Environmental Risk Points	0.1027 (0.0530–0.1600)	
			Vegetation Cover	0.0713 (0.0309–0.1500)	
			Land Use Type	0.0857 (0.0394–0.1200)	
		Socioeconomic vulnerability	Fiscal Revenue of the Administrative District	0.0812 (0.0212–0.2830)	
			Population Density	0.0792 (0.0300–0.2010)	
			Exposure	Heritage Value	0.7952 (0.7500–0.8330)
				Heritage Scale	0.2048 (0.1670–0.2500)

approaching 33 °C. Under the SSP2-4.5 scenario (Fig. 3e), temperatures in these regions increase by approximately 2 °C. In the SSP5-8.5 scenario (Fig. 3f), most plain areas exceed 35 °C, with localized zones approaching 36 °C. Both the frequency and intensity of extreme heat events are projected to rise substantially, posing significant thermal stress risks to heat-sensitive heritage, such as wooden structures and rammed-earth sites.

Figure 4 illustrates the comparison of precipitation under different climate scenarios. During the historical period, the spatial pattern of annual mean precipitation (Fig. 4a) displays a “higher in the southwest, lower in the northeast” distribution, with southwestern mountainous regions, such as Fangshan and Mentougou, receiving 600–650 mm annually. Under future scenarios, precipitation is projected to increase overall, with more pronounced increments under the high-emission pathway. Specifically, under the SSP2-4.5 scenario (Fig. 4b), increases in the southwestern mountains and southeastern plains range from 50 to 150 mm, whereas under the SSP5-8.5 scenario (Fig. 4c), localized increments exceed 200 mm. For maximum annual mean precipitation (Fig. 4d), high values during the historical period are concentrated in the southwestern mountain valleys, reaching approximately 800 mm. Under the SSP2-4.5 scenario (Fig. 4e), the high-precipitation zones expand; under the SSP5-8.5 scenario (Fig. 4f), they extend markedly into the plain districts of Fengtai, Daxing, and Tongzhou, with localized values exceeding 1000 mm, nearly double the historical levels. Such short-duration, high-intensity precipitation events are highly likely to trigger flooding and secondary geological hazards, posing significant risks of surface erosion and foundation scouring for permeable heritage structures, including stone carvings and masonry.

Exposure. In this study, exposure is defined as a weighted combination of heritage value and site scale, comprehensively capturing the social-historical significance and the physical-spatial susceptibility of the heritage system, thereby constituting a key component of climate risk assessment.

Cultural value reflects the historical significance, artistic merit, and societal influence of heritage sites, serving as a key basis for determining protection levels and allocating management resources.

Typically, cultural heritage value decreases progressively from national-level to municipal-level, district-level, and district-wide surveyed sites. This study calculates the proportions of these heritage categories in Beijing as 1:1.8:5.4:16.4. Under the assumption of equal total cultural value across levels, corresponding weights are derived and presented in Table 2. This weighting system reflects the increased potential exposure of higher-level heritage sites, attributable to their irreplaceable cultural value and greater restoration challenges. In the GIS-based spatial analysis, each site is assigned a value based on its protection level and spatially represented, thereby providing discrete data inputs for the exposure model.

The heritage scale defines the spatial extent of a site in geographic space. Larger areas are associated with higher structural complexity, greater microclimatic diversity, and wider potential pathways for climate impacts, thus increasing exposure⁴⁵. In this study, boundaries of national-level and municipal-level heritage units were extracted from the Beijing Cultural Heritage Map, and their areas were calculated using a GIS platform. Sites were then classified into graded intervals based on area, with the assigned values presented in Table 3.

Vulnerability. Vulnerability measures the sensitivity and adaptive capacity of cultural heritage to climatic disturbances, reflecting the compound property of whether a heritage asset can resist the shock and, if impacted, whether it can recover effectively^{46,47}. In this study, vulnerability is defined as the system’s response capacity, shaped by the interplay of the heritage’s intrinsic attributes, its surrounding natural environment, and the prevailing socio-economic and management conditions.

Intrinsic vulnerability characterizes the responsiveness of cultural heritage to climatic stressors based on its antiquity and material composition. In this study, the construction era of heritage assets is categorized into five chronological stages, ranging from the Pre-Qin period to the modern era. Older heritage sites exhibit greater susceptibility to long-term natural weathering and structural fatigue^{18,48}; therefore, higher vulnerability values are assigned to earlier periods (Table 4). This chronological classification

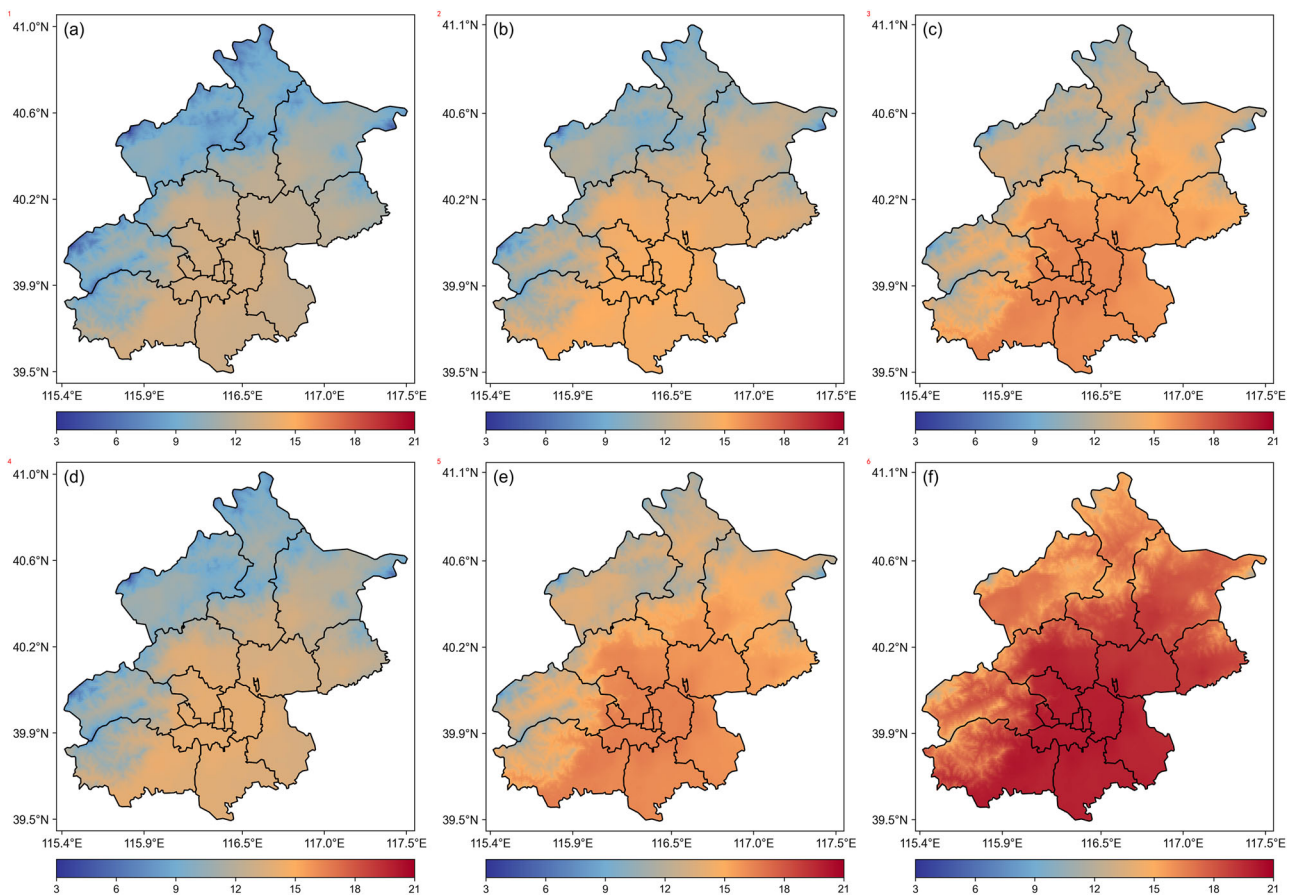


Fig. 3 | Comparison of temperature under different climate scenarios. a Annual mean temperature during the historical period (1901–2022); **b** Annual mean temperature under the SSP2-4.5 scenario (2023–2100); **c** Annual mean temperature under the SSP5-8.5 scenario (2023–2100); **d** Maximum annual mean temperature during the historical period (1901–2022); **e** Maximum annual mean temperature under the SSP2-4.5 scenario (2023–2100); **f** Maximum annual mean temperature under the SSP5-8.5 scenario (2023–2100).

reflects the general trend of deterioration. Given variations in architectural styles, material systems, and construction techniques, significant differences in vulnerability may exist among individual cultural heritage sites.

The materials used in cultural heritage can be broadly categorized into five types: timber, stone, brick, earth, and concrete. Due to differences in water resistance, pore structure, and other intrinsic properties, the climate-induced vulnerability of these materials varies significantly. Water resistance decreases in the following order: stone, concrete, brick, timber, and earth, indicating that stone and concrete are generally more resistant to precipitation-induced soaking damage than timber and earth. The porosity of timber and earth typically exceeds that of brick, concrete, and stone, making wood and earth more susceptible to moisture-related environmental stressors. Furthermore, the organic nature of timber renders it prone to fungal degradation, while the calcium-rich composition of stone increases its vulnerability to bio-corrosion by calciphilic organisms⁴⁹. For earthen sites, biological damage is primarily caused by the mechanical disruption from plant root growth on ancient structures. A comprehensive assessment indicates that rainfall vulnerability decreases approximately in the sequence: earth, timber, brick, stone, and concrete⁵⁰. The existing literature⁵⁰ analyzed the material composition of 1500 national and provincial-level cultural heritage sites, calculated the proportion of each material within different heritage categories, and derived corresponding material vulnerability levels for heritage types. This study adopts their findings to assign material-based vulnerability scores to cultural heritage assets, as presented in Table 5. Overall, the sites of ancient culture are predominantly composed of earth materials, which confer the highest level of vulnerability. In contrast, modern and contemporary buildings are primarily constructed using more

durable materials such as brick, stone, and concrete, resulting in relatively lower vulnerability. Ancient tombs contain a significant proportion of earthen structural components, making them more vulnerable than ancient architectural structures built from wood and brick.

Environmental vulnerability refers to the degree to which natural geographic conditions surrounding cultural heritage sites either exacerbate or mitigate the impacts of climate-related events^{51,52}. To assess this vulnerability, this study integrates four key indicators into the modeling framework: slope, distance to geological hazard points, vegetation cover as measured by the Normalized Vegetation Index (NDVI), and land-use type.

Topography is a critical determinant of environmental stability for cultural heritage. Among its parameters, slope provides a direct measure of terrain steepness and is strongly associated with the risk of landslides and debris flows, making it an essential indicator of vulnerability in the modeling framework^{53,54}. This study employs 30-meter resolution digital elevation model (DEM) data to compute the slope distribution across Beijing. Vegetation cover, quantified by the NDVI, serves as a measure of ecosystem resilience; higher NDVI values indicate greater environmental regulatory capacity and are associated with reduced vulnerability, thus classifying it as a negative vulnerability indicator. Land use types serve as proxies for biodiversity and the intensity of biological activities. Microbial activity can induce physical structural changes in cultural heritage, including expansion, contraction, and cracking, and can also promote chemical processes such as corrosion and mold formation⁵⁵. Similarly, animal activity poses significant threats to cultural heritage. Overall, regions with higher biological activity exhibit greater environmental vulnerability. Based on this relationship, vulnerability weights are assigned to different land use categories, as

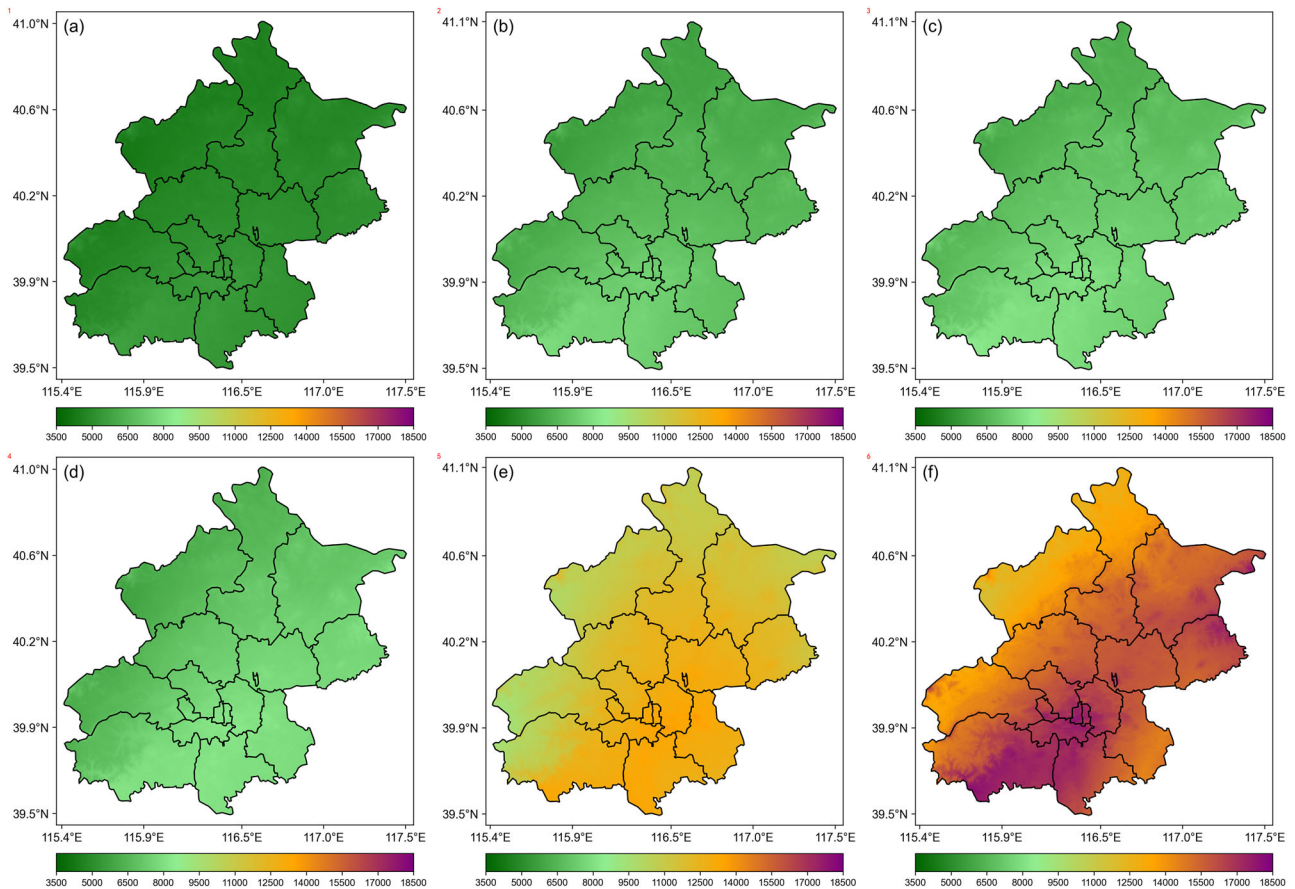


Fig. 4 | Comparison of precipitation under different climate scenarios. a Annual mean precipitation during the historical period (1901–2022); **b** Annual mean precipitation under the SSP2-4.5 scenario (2023–2100); **c** Annual mean precipitation under the SSP5-8.5 scenario (2023–2100); **d** Maximum annual mean precipitation

during the historical period (1901–2022); **e** Maximum annual mean precipitation under the SSP2-4.5 scenario (2023–2100); **f** Maximum annual mean precipitation under the SSP5-8.5 scenario (2023–2100).

Table 2 | Weights of cultural heritage value across different protection levels

Level	National-level	Municipal-level	District-level	District-wide survey
Weight	0.55	0.31	0.1	0.04

summarized in Table 6. Forests are assigned the highest weight, followed by grasslands and water bodies, whereas urban, industrial, and residential land receive the lowest weight.

The distance to geological hazard sources is used to assess the spatial pressure imposed by debris flows, landslides, ground subsidence, and collapses on cultural heritage sites. To quantitatively evaluate the geological hazard risks facing heritage assets, this study employs GIS-based spatial analysis to calculate the distance from each heritage site to the nearest hazard location. The shorter the distance to geological hazard sources, the higher the vulnerability value assigned to cultural heritage sites.

Socioeconomic vulnerability reflects spatial disparities in heritage protection resources and management capacity, primarily indicated by the potential for fiscal and human resource investment⁵⁶. Fiscal revenue serves as a critical enabler for the routine maintenance and disaster response of cultural heritage, ensuring the sustained implementation of conservation measures and timely intervention during emergencies. Significant disparities exist in fiscal revenue levels across Beijing’s districts. In 2023, the public budget revenues of Chaoyang, Haidian, and Xicheng Districts exceeded 40 billion yuan, whereas those of Yanqing, Mentougou, Huairou,

Pinggu, and Miyun remained below 4.5 billion yuan. For the large number of district-level and district-wide surveyed cultural heritage sites, higher revenue districts are able to allocate substantially greater resources toward maintenance, restoration, and disaster prevention. In contrast, lower-revenue districts face persistent underfunding in heritage conservation, leading to limited protective capacity and heightened vulnerability.

The 3-kilometer buffer distance corresponds to the typical spatial extent of a rural settlement in the Beijing context, reflecting the scale at which local communities engage in daily activities and interact with their surrounding environment. When a heritage site is located far from human settlements such as villages, the absence of nearby residents restricts regular monitoring of its condition, thereby increasing its susceptibility to undetected deterioration or intentional damage. Conversely, higher population density within the same radius facilitates sustained on-site observation and informal protection through active community involvement. In Beijing, the population distribution is highly uneven, with dense concentrations in the urban core and southeastern plain regions, while the northwest mountainous areas are sparsely populated. As a result, cultural heritage sites in these peripheral, low-density areas are more likely to be socially marginalized and receive insufficient institutional or public attention, leading to elevated levels of vulnerability.

Results

Risk comparison between different climate scenarios

Climate risks to Beijing’s cultural heritage under two future climate scenarios (SSP2-4.5 and SSP5-8.5) for the period 2021–2100 were

quantitatively assessed, as illustrated in Fig. 5. Overall, transitioning from the SSP2-4.5 to the SSP5-8.5 scenario results in a substantial increase in climate risks across all cultural heritage sites. Under the SSP2-4.5 scenario, the mean risk value for Beijing’s cultural heritage is 0.223, with a range of 0.052–0.545. In contrast, under the SSP5-8.5 scenario, the average risk increases to 0.315, spanning from 0.119 to 0.723, reflecting an approximate 41.5% rise in overall risk levels.

The regions experiencing the most rapid increase in climate risks are primarily concentrated in Tongzhou, Xicheng, Fengtai, Haidian, and Yanqing. Among these, 16 district-level surveyed cultural relics, including Nangao Guan Di Temple (Chaoyang), Jingling Shengongjian (Changping), Dashengling Reservoir (Yanqing), and Mituo Temple (Xicheng), have experienced risk increases exceeding 100%, identifying them as priority sites requiring monitoring and targeted adaptation measures. In contrast, national-level heritage sites such as the Tongzhou section of the Grand Canal (Tongzhou), Shichahai (Xicheng), the Temple of Heaven (Dongcheng), and the Forbidden City (Dongcheng) exhibit relatively moderate risk increases, ranging from 20% to 24%. Nonetheless, even these less pronounced changes highlight the widespread and systemic nature of climate risk impacts across all levels of cultural heritage.

Risk comparison across different levels of heritage

The climate risks across cultural heritage sites of varying protection levels are compared in Fig. 6. Under both the SSP2-4.5 and SSP5-8.5 scenarios, average climate risk exhibits a consistent decline from national-level to municipal-, district-, and district-wide surveyed heritage. However, when examining the magnitude of climate risk changes across scenarios, a clear ascending trend emerges, from national-level to municipal-, district-, and

Table 3 | Weights of the cultural heritage scale across different area ranges

Area Range (m ²)	Weight
<500	0.2
500–5000	0.4
5000–50,000	0.6
50,000–500,000	0.8
>500,000	1

Table 4 | Vulnerability weights of cultural heritage across different chronological classifications

Era	Pre-Qin	Qin–Sui	Tang–Yuan	Ming–Qing	Modern and contemporary
Weight	1.0	0.8	0.6	0.4	0.2

Table 5 | Material composition-based vulnerability weights for five types of cultural heritage

Heritage type	AAS	AT	IMACHSTB	SOAC	CTASC
Weight	0.628	0.736	0.515	0.812	0.599

AAS the ancient architectural structures, AT the ancient tombs, IMACHSTB the important modern and contemporary historic sites and the typical buildings, SOAC the sites of ancient culture, CTASC the cave temples and stone carvings. The table is derived from literature⁵⁰.

Table 6 | Vulnerability weights of cultural heritage across different land-use types

Land-use type	Forest land	Grassland	Water bodies	Agricultural land	Future development land	Urban, industrial, and residential land
Weight	0.9	0.8	0.7	0.6	0.4	0.2

district-wide surveyed heritage. This indicates that while lower protection level heritage sites currently face lower average climate risks, they experience greater relative increases under higher-emission conditions. Specifically, the escalation in climate risk from SSP2-4.5 to SSP5-8.5 becomes progressively more pronounced as protection level decreases, highlighting the heightened vulnerability of less protected cultural heritage to future climate change impacts.

Cultural heritage sites within the same protection level exhibit substantial internal variation. Among these, district-wide surveyed heritage displays the largest inter-group differences, whereas national-level heritage shows the smallest; as protection level increases, inter-group variability systematically decreases. Under the SSP2-4.5 scenario, the standard deviations of climate risk for national-level, municipal-level, district-level, and district-wide surveyed heritage are 0.0271, 0.0309, 0.0315, and 0.0453, respectively. Under the SSP5-8.5 scenario, these values increase to 0.0373, 0.0371, 0.0426, and 0.0583, respectively. This indicates that from SSP2-4.5 to SSP5-8.5, inter-group differences in climate risk across protection levels widen, particularly for lower level heritage categories.

Risk comparison across different types of heritage

Figure 7 presents the distribution of climate risks across different types of cultural heritage. The climate risks exhibit a bimodal pattern, primarily driven by the hierarchical grade of heritage sites. Within each heritage type, national-level and municipal-level sites face significantly higher risks than their district-level and district-wide surveyed counterparts. Despite this dominant influence of protection hierarchy, notable differences in climate risk persist across heritage types. Overall, median risk levels decrease in the following order: ancient architectural structures (AAS), cave temples and stone carvings (CTASC), important modern and contemporary historic sites and typical buildings (IMACHSTB), ancient tombs (AT), and sites of ancient culture (SOAC).

Risk comparison across different regions

Figure 8 illustrates the spatial distribution of climate risks across different regions. Yanqing District exhibits the highest climate risk, followed by Mentougou, Dongcheng, Xicheng, Haidian, Changping, and Fangshan Districts. These areas are primarily located in Beijing’s western mountainous regions and central urban core, encompassing major cultural heritage zones such as the Great Wall Cultural Belt, the West Mountain and Yongding River Cultural Belt, and the Three Mountains and Five Gardens Cultural Zones. In the mountainous west, both climate hazards and the intrinsic vulnerability of cultural heritage are elevated due to exposure to extreme precipitation, temperature fluctuations, and geological sensitivity. In contrast, regions with lower climate risks, including Shunyi, Daxing, Huairou, Chaoyang, and Fengtai Districts, are mainly concentrated in the central and southeastern parts of the city, where the density of national- and municipal-level heritage sites is relatively low.

Sensitivity analysis

Climate risk assessment for cultural heritage involves numerous parameters, among which the assignment of weights is subject to considerable uncertainty. To address this, the study employs the Monte Carlo method by modeling expert-derived weight values as normally distributed variables and conducting 5000 resampling iterations to evaluate the robustness of the assessment results, as illustrated in Fig 9. Although variations in parameter weights lead to changes in the absolute values of risk indices, the overall risk structure remains stable. Under the SSP2-4.5 scenario, the mean climate risk for Beijing’s cultural heritage is 0.223, with an average confidence interval

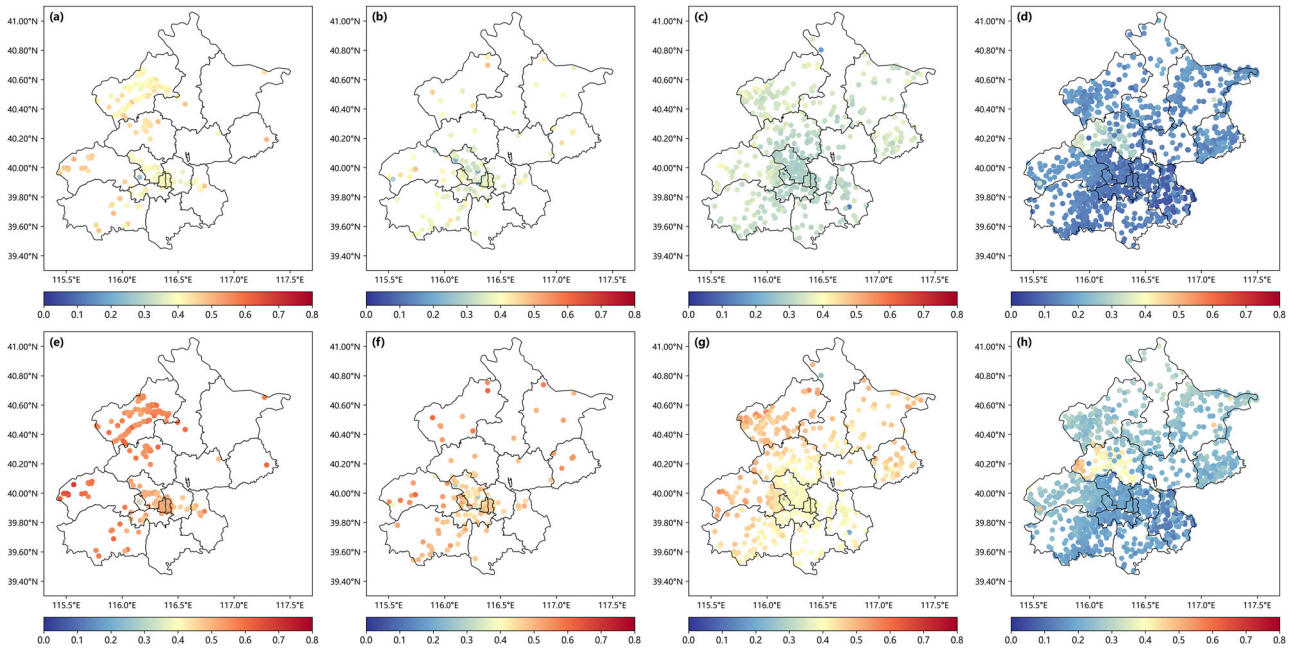
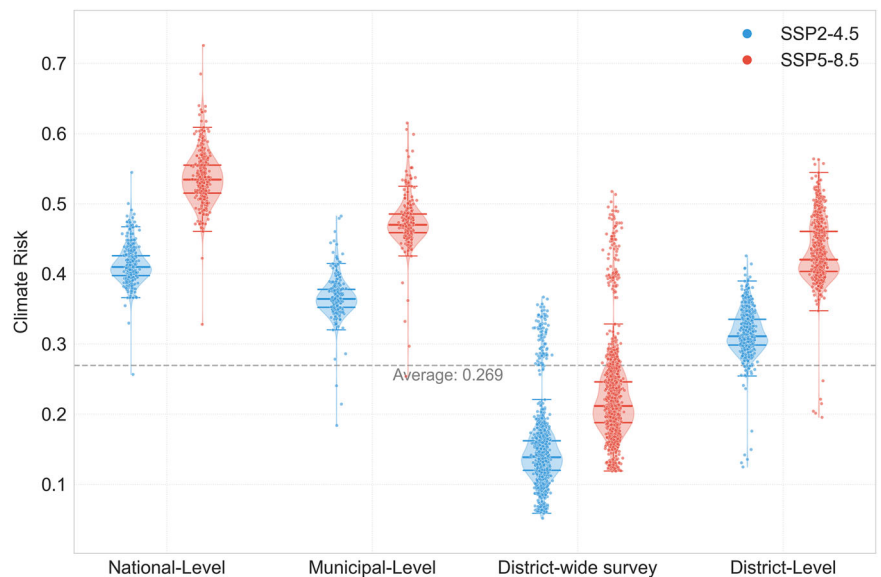


Fig. 5 | Climate risk comparison across different protection levels between the ssp2-4.5 and ssp5-8.5 scenarios. **a** Climate risk of National-Level cultural heritage under the SSP2-4.5 scenario; **b** Climate risk of Municipal-Level cultural heritage under the SSP2-4.5 scenario; **c** Climate risk of District-Level cultural heritage under the SSP2-4.5 scenario; **d** Climate risk of District-wide surveyed cultural heritage

under the SSP2-4.5 scenario; **e** Climate risk of National-Level cultural heritage under the SSP5-8.5 scenario; **f** Climate risk of Municipal-Level cultural heritage under the SSP5-8.5 scenario; **g** Climate risk of District-Level cultural heritage under the SSP5-8.5 scenario; **h** Climate risk of District-wide surveyed cultural heritage under the SSP5-8.5 scenario.

Fig. 6 | Risk comparison across different levels of heritage under different scenarios. This figure presents the climate risks faced by cultural heritage sites at different protection levels under the SSP2-4.5 and SSP5-8.5 scenarios. Blue denotes the SSP2-4.5 scenario, while red denotes the SSP5-8.5 scenario. The central horizontal line represents the mean value, along with the 25th and 75th percentile risk intervals.



width of 0.115 at the 95% confidence level. The average Spearman rank correlation coefficient between the reweighted risk rankings and the original rankings reaches 0.989, indicating strong rank consistency. Under the SSP5-8.5 scenario, the mean risk increases to 0.315, with an average 95% confidence interval width of 0.132, and the corresponding Spearman correlation coefficient is 0.991, further confirming the stability of the risk hierarchy despite parameter uncertainty.

In both scenarios, high-risk areas remain consistently concentrated in the urban core and the northwestern mountainous regions, while low-risk areas are predominantly located in the eastern plain. No large-scale spatial reconfiguration is observed. The high Spearman correlation coefficients and narrow confidence intervals indicate that the relative

risk gradient is robust to parameter uncertainty. This sensitivity analysis demonstrates that the risk assessment results are reliable enough to support the identification and prioritization of high risk zones for cultural heritage conservation.

However, it should be noted that beyond indicator weights, this study is subject to multiple sources of uncertainty. First, future climate conditions over the coming century remain inherently unpredictable⁵⁷. Although climate models have undergone continuous improvements over recent decades, they still exhibit intrinsic uncertainties in simulating complex climatic processes. Moreover, the assessment relies on annual mean temperature and precipitation as proxies for climate risk, introducing uncertainty due to the omission of short-duration extreme

Fig. 7 | Risk comparison across different types of heritage under different scenarios. This figure presents the climate risks faced by different types of cultural heritage sites under the SSP2-4.5 and SSP5-8.5 scenarios. Blue denotes the SSP2-4.5 scenario, while red denotes the SSP5-8.5 scenario. The central horizontal line represents the mean value, along with the 25th and 75th percentile risk intervals. AAS refers to ancient architectural structures, AT refers to ancient tombs, IMACHSTB refers to important modern and contemporary historic sites and typical buildings, SOAC refers to sites of ancient culture, CTASC refers to cave temples and stone carvings.

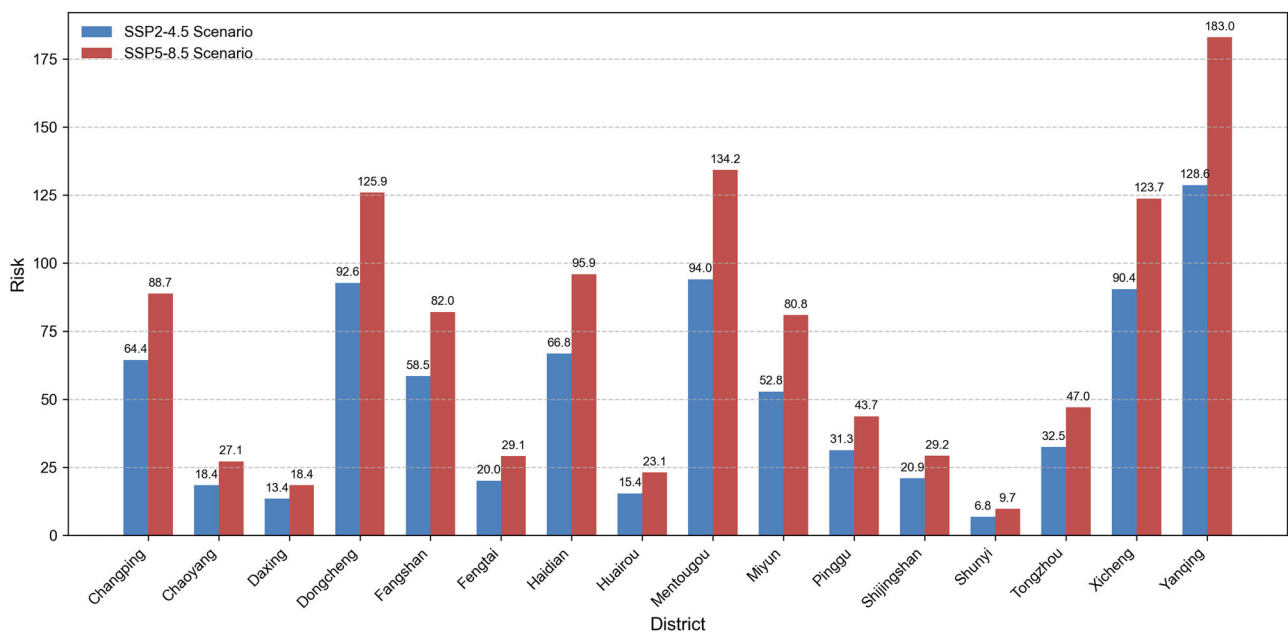
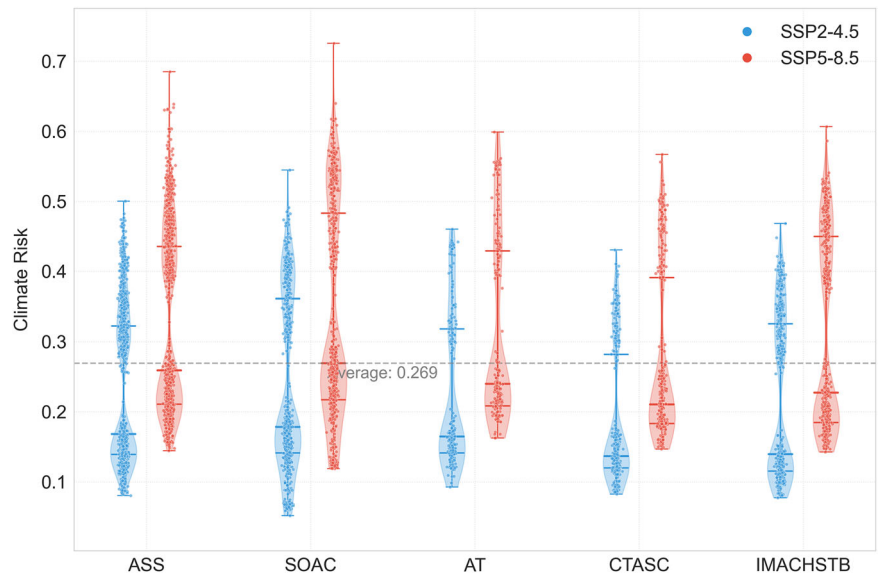


Fig. 8 | Total climate risk values at the district scale for cultural heritage sites. This figure presents the climate risks faced by cultural heritage sites in 16 districts of Beijing under the SSP2-4.5 and SSP5-8.5 scenarios. Blue denotes the SSP2-4.5 scenario, while red denotes the SSP5-8.5 scenario.

events. Second, the quantification of several indicators involves subjective assumptions, such as the valuation of cultural heritage based on its protection level or the assignment of vulnerability scores according to the age of heritage assets, both of which entail a degree of epistemic uncertainty. Third, the analysis focuses exclusively on direct climate risks and does not account for indirect risks. Climate-induced systemic changes in socio-economic systems, such as shifts in land use, population dynamics, and resource allocation, may impose additional pressures on cultural heritage conservation, yet these cascading effects are not captured within the current framework.

Despite uncertainties, this study advances the understanding of climate risks to Beijing’s cultural heritage. The results provide a comparative basis for assessing risks across districts and heritage types, enabling more effective prioritization and improved allocation of conservation resources. As a macro-scale analysis, the findings represent

aggregate patterns rather than site-specific conditions and should not be used to explain climate risks for individual heritage sites.

Discussion

The findings of the risk assessment offer critical policy insights to guide decision-makers in designing and implementing effective adaptation strategies in response to climate change. Existing research has identified a range of adaptive measures to address the threats posed by climate change to cultural heritage protection, including technological solutions, behavioral modifications, management strategies, and policy instruments^{58,59}. As a macro-level assessment, this study is not intended to analyze site-specific risks for individual heritage sites, but rather to compare climate-related risks across multiple heritage locations, thereby underscoring the importance of prioritizing climate risk management. These findings carry significant policy

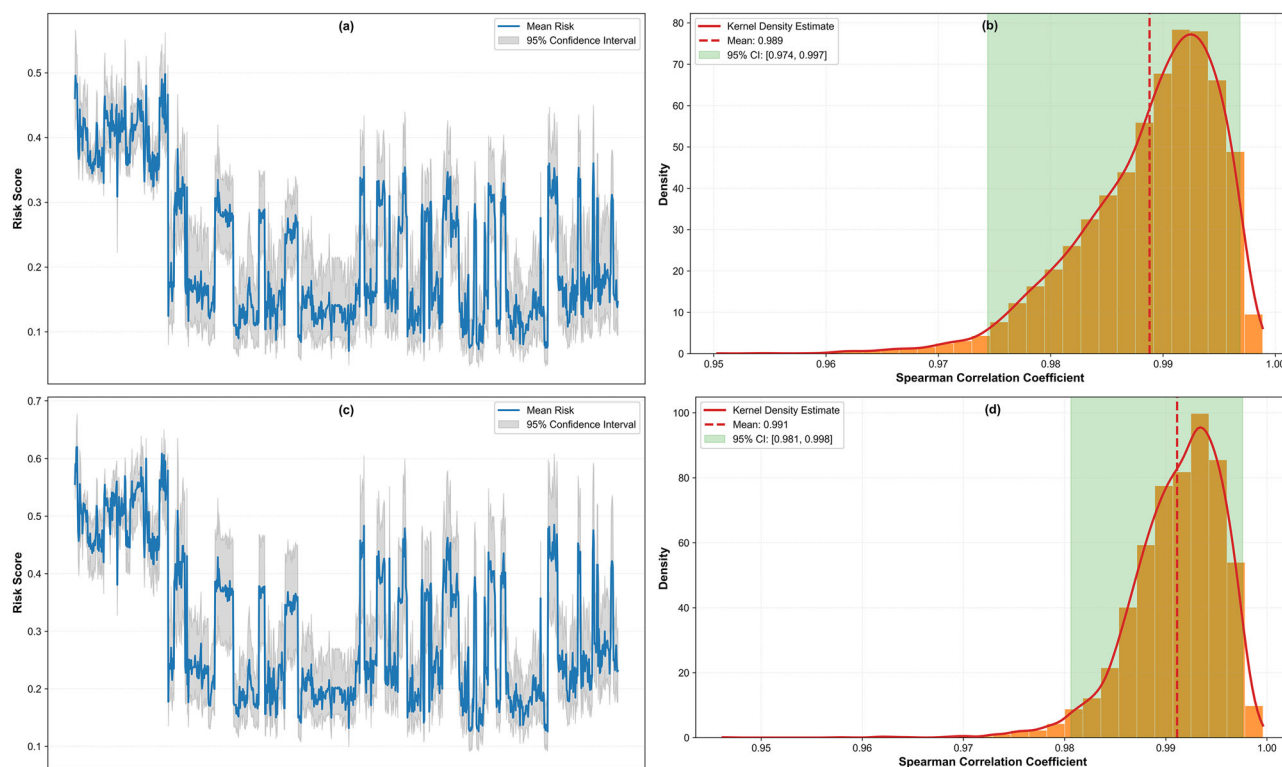


Fig. 9 | Results of the sensitivity analysis for climate risk. a Mean Risk Confidence Intervals under the SSP2-4.5 scenario; **b** Ranking Stability Analysis under the SSP2-4.5 scenario; **c** Mean Risk Confidence Intervals under the SSP5-8.5 scenario; **d** Ranking Stability Analysis under the SSP5-8.5 scenario.

implications for enhancing cultural heritage management practices in Beijing and across China.

First, enhancing greenhouse gas emission reduction represents a fundamental pathway for mitigating climate risks to cultural heritage

The risk assessment results indicate that climatic forcing is the primary driver of climate-related risks to cultural heritage in Beijing. Under the high-emission scenario (SSP5-8.5), overall climate risk increases by 41.5% compared to the medium-emission scenario (SSP2-4.5), highlighting the dominant influence of future emission trajectories on heritage risk outcomes. These findings underscore the necessity of enhancing global greenhouse gas (GHG) emission reduction. Although most countries have established Nationally Determined Contributions and implemented various mitigation measures, current global emission trends remain more closely aligned with high-emission pathways than with stabilization scenarios such as SSP2-4.5^{10,60}. From a cultural heritage perspective, this divergence implies a growing baseline level of climate risk, even under improved local management conditions. Consequently, heritage protection cannot be decoupled from broader climate governance, and there is an urgent need for strengthened global mitigation efforts to address climate risks at their source⁵².

Second, developing adaptation plans constitutes a proactive strategy for mitigating climate risks

In recent years, Beijing has increasingly integrated climate change considerations into the risk management of cultural heritage. However, the current focus remains primarily on post-disaster emergency responses and protective restoration efforts. The existing planning requirements for systematic cultural relic protection, such as the “Requirements for the Preparation of Protection Plans for National Key Cultural Relics Protection Units”, mainly emphasize value assessment, management assessment, current situation assessment, and utilization assessment. Although environmental factors are included in the current situation assessment, there is a

lack of dedicated evaluation mechanisms addressing the diverse adverse impacts of climate change. Similarly, current national strategic plans on climate change adaptation have not adequately incorporated cultural heritage concerns. For instance, the “National Adaptation Strategy to Climate Change 2035” released in June 2022 only briefly refers to cultural heritage in the context of climate resilient tourism, recommending scientifically guided human interventions for the protection of ancient trees, bridges, villages, and historic buildings as tourism resources, without fully recognizing cultural heritage as a key domain within national climate adaptation frameworks. The study advocates a transition from reactive responses to proactive and planned adaptation strategies, which are essential for enhancing the resilience of cultural heritage sites to future climate conditions. Proactive adaptation measures include strengthening the monitoring of cultural heritage assets, conducting scientific assessments of climate change impacts, and developing cultural heritage-specific climate risk maps; formulating a comprehensive climate risk management manual tailored to different protection levels and types of cultural heritage to guide targeted adaptation actions; and selecting representative heritage sites as pilot projects to promote diversified adaptation practices across the broader heritage network.

Third, implementing differentiated adaptation actions constitutes a strategic approach under resource constraints

Risk assessment results demonstrate that cultural heritage exhibits significant variations in risk levels across different administrative levels, types, and geographic regions. From a governmental perspective, given the limited availability of funds to support high cost adaptation measures across all areas, it is strategically prudent to develop feasible solutions and differentiated adaptation pathways based on distinct risk profiles. At the individual site level, national-level heritage sites and large scale heritage areas tend to face heightened climate risks^{1,61}. Therefore, specialized climate risk response mechanisms should be established for high value cultural heritage, encompassing priority access to financial resources, deployment of high precision climate monitoring and assessment technologies, and implementation of preventive conservation measures. District-level and district-

wide surveyed heritage constitute a collectively vulnerable group within the broader cultural heritage system. Particularly in transitional zones between urban fringes and mountainous regions, these sites face compounded environmental pressures and governance gaps. For heritage sites that are numerous yet carry lower protection designations, enhancing public participation and community-based governance is essential. Engaging stakeholders in long-term stewardship can help bridge the disparity between government funding and risk exposure, thereby strengthening the resilience and long-term adaptive capacity of the entire heritage system.

Data availability

The datasets generated and/or analyzed during the current study are not publicly available due to the protection of cultural properties, but are available from the corresponding author on reasonable request.

Received: 7 October 2025; Accepted: 4 March 2026;

Published online: 13 March 2026

References

1. Nguyen, K. N. & Baker, S. Climate change impacts on UNESCO World heritage-listed cultural properties in the Asia–Pacific region: a systematic review of state of conservation reports, 1979–2021. *Sustainability* **15**, 14141 (2023).
2. Sesana, E., Gagnon, A. S., Ciantelli, C., Cassar, J. & Hughes, J. J. Climate change impacts on cultural heritage: a literature review. *Wiley Interdiscip. Rev. Clim. Change*. **12**, <https://doi.org/10.1002/wcc.710> (2021).
3. Sesana, E., Gagnon, A. S., Bertolin, C. & Hughes, J. Adapting cultural heritage to climate change risks: perspectives of cultural heritage experts in Europe. *Geosci* **8**, 305–305 (2018).
4. Fatorić, S. & Biesbroek, R. Adapting cultural heritage to climate change impacts in the Netherlands: barriers, interdependencies, and strategies for overcoming them. *Clim. Change* **162**, 301–320 (2020).
5. Fatorić, S. & Daly, C. Towards a climate-smart cultural heritage management. *Wiley Interdiscip. Rev. Clim. Change*. **14**, <https://doi.org/10.1002/wcc.855> (2023).
6. Reimann, L., Vafeidis, A. T., Brown, S., Hinkel, J. & Tol, R. S. J. Mediterranean UNESCO World Heritage at risk from coastal flooding and erosion due to sea-level rise. *Nat. Commun.* **9**, <https://doi.org/10.1038/s41467-018-06645-9> (2018).
7. Xiao, X. et al. Optimizing historic preservation under climate change: decision support for cultural resource adaptation planning in national parks. *Land Use Policy* **83**, 379–389 (2019).
8. Brimblecombe, P. & Richards, J. Applied climatology for heritage. *Theor. Appl. Climatol.* **155**, 7325–7333 (2024).
9. Orr, S. A., Richards, J. & Fatorić, S. Climate change and cultural heritage: a systematic literature review (2016–2020). *Historic Environ. Policy Pract.* **12**, 434–477 (2021).
10. IPCC. *IPCC, 2023: Climate Change 2023: Synthesis Report, Summary for Policymakers. Contribution of Working Groups I, II, and III to the Sixth Assessment Report of the Intergovernmental Panel on Climate Change* Core Writing Team, H. Lee and J. Romero (eds.) <https://doi.org/10.59327/ipcc/ar6-9789291691647.001> (IPCC, 2023).
11. UNESCO. *UNESCO Strategy for Action on Climate Change*. The 39th general conference of UNESCO (UNESCO, 2017).
12. UNESCO. *Managing Disaster Risks for World Heritage* (The workshops of UNESCO, 2010).
13. Lu, Y., Han, Q., Zhang, Z., Sun, Z. & Dai, J. Spatiotemporal distribution and evolution of global world cultural heritage, 1972–2024. *ISPRS Int. J. Geo Inf.* **14**, 190–190 (2025).
14. Li, Q., Zhang, T., Fang, Y. & Lin, F. A pathological diagnostic method for traditional brick-masonry dwellings: a case study in guangfu ancient city. *Buildings* **14**, 3563 (2024).
15. Grossi, C. M., Brimblecombe, P. & Harris, I. Predicting long term freeze–thaw risks on Europe built heritage and archaeological sites in a changing climate. *Sci. Total. Environ.* **377**, 273–281 (2007).
16. Nava, S. et al. An integrated approach to assess air pollution threats to cultural heritage in a semi-confined environment: the case study of Michelozzo’s Courtyard in Florence (Italy). *Sci. Total. Environ.* **408**, 1403–1413 (2010).
17. Bonazza, A. et al. Did smoke from the Kuwait oil well fires affect Iranian archaeological heritage. *Environ. Sci. Technol.* **41**, 2378–2386 (2007).
18. Esteban-Cantillo, O. J., Menendez, B. & Quesada, B. Climate change and air pollution impacts on cultural heritage building materials in Europe and Mexico. *Sci. Total. Environ.* **921**, 170945 (2024).
19. Hu, H. & Hewitt, R. J. Understanding climate risks to world cultural heritage: a systematic analysis and assessment framework for the case of Spain. *Herit Sci.* **12**, <https://doi.org/10.1186/s40494-024-01299-x> (2024).
20. Sardella, A. et al. Risk mapping for the sustainable protection of cultural heritage in extreme changing environments. *Atmosphere* **11**, 700 (2020).
21. Bonazza, A. & Sardella, A. Climate change and cultural heritage: methods and approaches for damage and risk assessment addressed to a practical application. *Heritage* **6**, 3578–3589 (2023).
22. Hu, H. & Hewitt, R. J. Future climate risks to world cultural heritage sites in Spain: a systematic analysis based on shared socioeconomic pathways. *Int. J. Disaster Risk. Reduct.* **113**, 104855 (2024).
23. Piao, J., Chen, W., Wang, L. & Chen, S. Future projections of precipitation, surface temperatures and drought events over the monsoon transitional zone in China from bias-corrected CMIP6 models. *Int. J. Climatol.* **42**, 1203–1219 (2021).
24. Jia, M. et al. Exploring the impact of climate change on flood risk at cultural heritage sites using a GIS-based SCS-CN method: a case study of Shanxi province, China. *Int. J. Disaster Risk. Reduct.* **96**, 103968–103968 (2023).
25. Liu, Y. et al. Flood risk assessment combining machine learning with multi-criteria decision analysis in Jiangxi Province, China. *Int. J. Disaster Risk Sci.* **16**, 858–869 (2025).
26. Han, Y. & Semnani, S. J. Important considerations in machine learning-based landslide susceptibility assessment under future climate conditions. *Acta Geotech.* **20**, 475–500 (2024).
27. Thomas, H., Marincioni, V. & Orr, S. A. Multi-determinant climate change risk assessment for heritage: a review of current approaches and future needs. *Clim. Risk Manag.* **49**, 100727 (2025).
28. Dimabayao, J. J., Lara, J. L., Canoura, L. G. & Solheim, S. Integrating climate risk in cultural heritage: a critical review of assessment frameworks. *Heritage* **8**, 312–312 (2025).
29. Fiorucci, M. et al. Machine learning for cultural heritage: a survey. *Pattern Recognit. Lett.* **133**, 102–108 (2020).
30. Nicu, C. Natural hazards—a threat for immovable cultural heritage: a review. *Int. J. Conserv. Sci.* **8**, 375–388 (2017).
31. Fatorić, S. & Egberts, L. Realising the potential of cultural heritage to achieve climate change actions in the Netherlands. *J. Environ. Manag.* **274**, 111107 (2020).
32. Crowley, K. et al. Cultural heritage and risk assessments: Gaps, challenges, and future research directions for the inclusion of heritage within climate change adaptation and disaster management. *Climate Resilience*. **1**, <https://doi.org/10.1002/cli2.45> (2022).
33. Phillips, H. The capacity to adapt to climate change at heritage sites—The development of a conceptual framework. *Environ. Sci. Policy* **47**, 118–125 (2015).
34. Richards, J. & Brimblecombe, P. The transfer of heritage modelling from research to practice. *Herit Sci.* **10**, <https://doi.org/10.1186/s40494-022-00650-4> (2022).
35. The National People’s Congress. *The Law of the People’s Republic of China on the Protection of Cultural Relics* (The National People’s Congress, 2024).
36. Gao, Y. et al. Preventive monitoring and study of insect damage of carpenter bees to timber components of Chinese historic buildings, Preventive Conservation - From Climate and Damage Monitoring to a

- Systemic and Integrated Approach. *Norwegian University of Science and Technology, Faculty of Humanities, Department of Interdisciplinary Studies of Culture* 87–91 (Taylor & Francis Group, 2020).
37. Ma, Y. et al. Water-related deterioration risk assessment for sustainable conservation of heritage buildings in the Forbidden City, China. *Dev. Built Environ.* **17**, 100293 (2024).
38. Wang, X., Meng, J., Zhu, T. & Zhang, J. Prediction of wind erosion over a heritage site: a case study of Yongling mausoleum, China. *Built Hérit* **3**, 41–57 (2019).
39. Richards, J. & Brimblecombe, P. Multi-model ensemble of frost risks across East Asia (1850–2100). *Clim. Change.* **177**, <https://doi.org/10.1007/s10584-024-03723-4> (2024).
40. Loli, A. & Bertolin, C. Indoor multi-risk scenarios of climate change effects on building materials in Scandinavian Countries. *Geoscience* **8**, 347–347 (2018).
41. Blavier, C. L. S. et al. Assessing climate impact on heritage buildings in Trentino—South Tyrol with high-resolution projections. *Atmosphere* **16**, 799 (2025).
42. Peng, S. Zhang 1-km monthly precipitation dataset for China (1901–2024). <https://doi.org/10.5281/zenodo.3114194> (2020).
43. Peng, S. 1-km monthly mean temperature dataset for China (1901–2024). <https://doi.org/10.11888/meteoro.tpcd.270961> (2019).
44. Peng, S. Zhang 1 km multi-scenario and multi-model monthly precipitation data for China (2021–2100). <https://doi.org/10.11866/db.ioess.2021.002> (2025).
45. Lankester, P. & Knight, R. Towards a national heritage climate change risk assessment hacia una evaluación del riesgo de cambio climático del patrimonio nacional. *Stud. Conserv.* **69**, 1–14 (2024).
46. Fabbicatti, K., Boissenin, L., & Citoni, M. Heritage Community Resilience: towards new approaches for urban resilience and sustainability. *City Territ Archit.* **7**, <https://doi.org/10.1186/s40410-020-00126-7> (2020).
47. Ravan, M., Revez, M. J., Pinto, I. V., Brum, P. & Birkmann, J. A vulnerability assessment framework for cultural heritage sites: the case of the Roman ruins of Tróia. *Int. J. Disaster Risk Sci.* **14**, 26–40 (2023).
48. Giglio, F., Frontera, P., Malara, A. & Armocida, F. Materials and climate change: a set of indices as the benchmark for climate vulnerability and risk assessment for tangible cultural heritage in Europe. *Sustainability* **16**, 2067 (2024).
49. Singh, J., Mann, P. & White, N. Timber decay: causes and remedies. *Struct. Eng. Int.* **6**, 200–202 (1996).
50. Wang, X., Li, H., Wang, Y. & Zhao, X. Assessing climate risk related to precipitation on cultural heritage at the provincial level in China. *Sci. Total Environ.* **835**, 155489 (2022).
51. Gkaifyllia, A., Hasiotis, T. & Tzoraki, O. Vulnerability of coastal heritage in the context of climate adaptation: a review. *Environ. Earth Sci. Proc.* **14**, <https://doi.org/10.3390/eesp2025032014> (2025).
52. Chen, Z. et al. World Cultural Heritage sites are under climate stress and no emissions mitigation pathways can uniformly protect them. *Commun. Earth Environ.* **6**, <https://doi.org/10.1038/s43247-025-02603-8> (2025).
53. Allam, A. M., Ibrahim, M. G. & Kanae, S., Sharaan, M. Evaluating flood and landslide hazards to cultural heritage sites in Historic Cairo. *Nat. Hazards.* <https://doi.org/10.1007/s11069-025-07401-1> (2025).
54. Bonini, J. E. et al. Assessing landslide susceptibility and dynamics at cultural heritage sites by integrating machine learning techniques and persistent scatterer interferometry. *Geomorphology* **469**, 109522–109522 (2024).
55. Dakal, T. C. & Cameotra, S. S. Microbially induced deterioration of architectural heritages: routes and mechanisms involved. *Environ. Sci. Eur.* **24**, <https://doi.org/10.1186/2190-4715-24-36> (2012).
56. Daly, C. et al. Climate change adaptation policy and planning for cultural heritage in low- and middle-income countries. *Antiquity* **96**, 1427–1442 (2022).
57. (IPCC), I.P. on C.C. *Climate Change 2021 – The Physical Science Basis* <https://doi.org/10.1017/9781009157896> (Cambridge University Press, 2023).
58. Fatorić, S. & Seekamp, E. Are cultural heritage and resources threatened by climate change? A systematic literature review. *Clim. Change* **142**, 227–254 (2017).
59. Blavier, C. L. S. et al. Adaptive measures for preserving heritage buildings in the face of climate change: a review. *Build. Environ.* **245**, 110832 (2023).
60. UNEP *Emissions Gap Report 2025: Off Target - Continued Collective inaction puts Global Temperature Goal at Risk*. UNEP. <https://wedocs.unep.org/handle/20.500.11822/48854> (2025).
61. Aktürk, G. & Hauser, S. J. Integrated understanding of climate change and disaster risk for building resilience of cultural heritage sites. *Nat. Hazards.* <https://doi.org/10.1007/s11069-024-06970-x> (2024).

Acknowledgements

This work was funded by the Beijing Municipal Social Science Foundation, grant number 22LSB008.

Author contributions

Li Huimin: Conceptualization, Funding acquisition, Methodology, Project administration, Resources, Validation, Writing—review and editing. Li Ruqi: Data curation, Formal analysis, Visualization, Writing—original draft.

Competing interests

The authors declare no competing interests.

Additional information

Correspondence and requests for materials should be addressed to Huimin Li.

Reprints and permissions information is available at <http://www.nature.com/reprints>

Publisher's note Springer Nature remains neutral with regard to jurisdictional claims in published maps and institutional affiliations.

Open Access This article is licensed under a Creative Commons Attribution-NonCommercial-NoDerivatives 4.0 International License, which permits any non-commercial use, sharing, distribution and reproduction in any medium or format, as long as you give appropriate credit to the original author(s) and the source, provide a link to the Creative Commons licence, and indicate if you modified the licensed material. You do not have permission under this licence to share adapted material derived from this article or parts of it. The images or other third party material in this article are included in the article's Creative Commons licence, unless indicated otherwise in a credit line to the material. If material is not included in the article's Creative Commons licence and your intended use is not permitted by statutory regulation or exceeds the permitted use, you will need to obtain permission directly from the copyright holder. To view a copy of this licence, visit <http://creativecommons.org/licenses/by-nc-nd/4.0/>.

© The Author(s) 2026